

Electronic structure and de Haas-van Alphen frequencies in KFe_2As_2 within LDA+DMFT

Steffen Backes, Daniel Guterding, Harald O. Jeschke, and Roser Valentí
*Institut für Theoretische Physik, Goethe-Universität Frankfurt,
 Max-von-Laue-Str. 1, 60438 Frankfurt am Main, Germany*

(Dated: March 28, 2014)

Recent density functional theory (DFT) calculations for KFe_2As_2 have shown to be insufficient to satisfactorily describe angle-resolved photoemission (ARPES) measurements as well as observed de Haas van Alphen (dHvA) frequencies. In the present work, we extend DFT calculations based on the full-potential linear augmented plane-wave method by dynamical mean field theory (DFT+DMFT) to include correlation effects beyond the local density approximation. Our results indicate that KFe_2As_2 is a moderately correlated metal with a mass renormalization factor of the Fe $3d$ orbitals between 1.6 and 2.7. Also, the obtained shape and size of the Fermi surface are in good agreement with ARPES measurements and we observe some topological changes with respect to DFT calculations like the opening of an inner hole cylinder at the Z point. As a result, our calculated dHvA frequencies differ greatly from existing DFT results and qualitatively agree with experimental data. On this basis, we argue that correlation effects are important to understand the -presently under debate- nature of superconducting state in KFe_2As_2 .

PACS numbers: 71.15.Mb, 71.18.+y, 71.27.+a, 74.70.Xa

I. INTRODUCTION

KFe_2As_2 is the hole-doped end member of the well-studied $\text{Ba}_{1-x}\text{K}_x\text{Fe}_2\text{As}_2$ family of iron based superconductors [1] and it features superconductivity at $T_c = 3.4\text{K}$ without the need for application of external pressure [2]. This material is presently under debate since the origin of the superconducting phase and the pairing symmetry are still unclear [3–5], both on the experimental and theoretical sides: Recent laser-based angle-resolved photoemission (laser ARPES) measurements found the superconducting order parameter to be of s -wave character with octet line-nodes [6], while a theoretical study [7] based on functional renormalization group considerations predicted a d -wave symmetry in agreement with measurements of thermal conductivity [8]. However, other theoretical studies [9, 10] based on spin pairing theory within the random phase approximation found that s - and d -wave pairing channels are strong competitors in electron-doped Fe-based systems and, therefore, both are possible in KFe_2As_2 . Moreover, transport measurements under pressure [11] suggested the presence of a possible phase transition from d -wave to s -wave around 1.75 GPa.

Also, strikingly, quantum oscillation experiments [12] predicted effective charge carrier masses of up to $19 m_e$ with an average mass enhancement factor m^*/m_{band} of about 9, while estimates from ARPES [13] and cyclotron resonance experiments [14] yield mass enhancement factors of about 3 for certain regions of the Fermi surface. On the theoretical side, density functional theory (DFT) calculations for KFe_2As_2 show poor agreement to ARPES data [13, 15, 16] and to de Haas-van Alphen frequencies [12, 17]. However, an existing DFT+DMFT study [18] for KFe_2As_2 suggested an improved comparison of the Fermi surface contour at $k_z=0$ with ARPES observations.

The importance of correlations in Fe-based superconductors has been pointed out in the past by numerous studies. A method that has proven to be quite successful in capturing the essential features of this class of correlated metals is DFT+DMFT [18–24]. Since an accurate knowledge of the electronic structure is essential for understanding both the normal and the superconducting state in Fe-based superconductors, we perform here a comprehensive LDA+DMFT investigation focused on features of the KFe_2As_2 compound that have not been dealt with in past studies[18]. We critically benchmark our theoretical results with ARPES and dHvA measurements to see in which way these results can improve our current understanding of this system.

II. METHODS

We combine density functional theory with dynamical mean-field theory in order to investigate the electronic structure and the resulting dHvA frequencies of KFe_2As_2 . Our calculations are based on the experimentally determined tetragonal $I4/mmm$ structures of KFe_2As_2 by Tafti *et al.* [25], which are given for pressure values starting at 0.23 GPa. We obtained a structure at zero pressure by linear extrapolation of the available data points. A comparison of this structure to the existing crystal structure by Rosza and Schuster [26] used in previous theoretical investigations, shows that while lattice parameters a , b , and c are consistent, the As z position differs significantly between both structures. The As z position was consistently determined over a large pressure range in the above mentioned study by Tafti *et al.* [25] and the As z position determined by Rosza and Schuster doesn't follow the trend shown by those data. Therefore we use the new structure with the following

parameters: $a = b = 3.8488 \text{ \AA}$, $c = 13.883 \text{ \AA}$, fractional As $z = 0.140663$.

For the DFT calculation we employed the full-potential linear augmented plane-wave (FLAPW) framework as implemented in WIEN2k [27], using the local density approximation (LDA) as well as the generalized gradient approximation (GGA) by Perdew, Burke and Ernzerhof [28] to the exchange-correlation functional. These calculations were converged self-consistently on a grid of 726 k points in the irreducible Brillouin zone. We performed calculations both, without and with inclusion of spin-orbit coupling (SO).

In order to include the effect of local correlations we employed fully charge self-consistent DMFT calculations, using modified routines from the WIEN2K code. We considered our implementation of the projection method from Bloch eigenstates to the correlated Fe $3d$ orbitals as described by Aichhorn *et al.* [29]. The energy window for the projection onto the localized basis was chosen comparatively large, ranging from -5 eV to 13 eV to capture the higher energy contribution of the Fe $3d$ orbitals to the density of states arising from the hybridization with the As $4p$ orbitals.

The DMFT impurity problem was solved using the continuous-time hybridization expansion quantum Monte Carlo solver in imaginary frequency space as implemented in the ALPS [30] code. We considered the Legendre polynomial representation [31] of the Green's function and improved estimators for the self-energy [32]. About 6×10^6 Monte-Carlo sweeps were performed at an inverse temperature $\beta = 40 \text{ eV}^{-1}$, corresponding to room temperature. The interaction parameters U and J were chosen as $U = 4 \text{ eV}$ and $J = 0.8 \text{ eV}$ in terms of Slater integrals and for the double-counting correction we used the fully-localized limit (FLL). All orbital characters presented here are defined in a coordinate system which is rotated by 45° around the crystallographic z axis, *i.e.* x and y are pointing along Fe-Fe nearest neighbor bonds. For determining the LDA+DMFT excitation energies that we used to define the Fermi surface, we tracked the maximum of the real-frequency spectral function throughout the Brillouin-zone. Analytic continuation of imaginary frequency data to the real frequency axis was performed by using the Padé approximation for the impurity self-energy and we checked the results against the stochastic maximum entropy method [33].

Two-dimensional cuts through the Fermi surface were extracted from WIEN2k on 200×200 k point grids for the LDA calculations. The Fermi surface was interpolated linearly.

De Haas-van Alphen frequencies were calculated from the electronic band structure using our own implementation of the dHvA frequency extraction algorithm by Rourke and Julian [34]. Band energies were extracted on grids spanning the reciprocal unit cell with 27648 k points for the DFT(+SO) setups and 50000 k points for the DMFT calculations. The frequency calculation was carried out on a $6.4 \cdot 10^7$ k point supercell grid contain-

ing 64 reciprocal unit cells. The higher k point density in the supercell compared to the input files is achieved by tricubic interpolation [35]. We align the supercell with a fictitious magnetic field vector, which allows us to investigate the angular dependence of dHvA frequencies. Here we varied the angle of the magnetic field from the (001) towards the (010) direction in reciprocal space. In order to calculate frequencies, the supercell is cut into one k point thick slices perpendicular to the vector of the magnetic field. On these slices a stepping algorithm detects crossings of the Fermi level between grid points and interpolates the position of the Fermi surface linearly. Point ordering is ensured within the stepping algorithm. If a closed orbit is detected, its area can be calculated from the geometry of the points unambiguously. The three-dimensional Fermi surface is reconstructed by matching orbits slice-by-slice. Only extremal orbits are singled out since non-extremal orbits do not contribute in experiment. De Haas-van Alphen frequencies are calculated for the extremal orbits and their positions are matched back to the reciprocal unit cell. Orbits with similar position and frequency are averaged.

III. RESULTS

A. Electronic structure

We first investigated the band structure of KFe_2As_2 obtained by the DFT calculation within LDA and LDA+SO. Results obtained with the GGA functional were nearly identical to the LDA result and are therefore not shown. At the Γ point (see Fig. 1 (a) and Fig. 2 (a)) we see three bands crossing the Fermi level, forming hole pockets of Fe $3d_{xy}$, $3d_{xz}$ and $3d_{yz}$ character. The two outer hole pockets form cylinders between the Γ and Z points, while the cylinder of the third inner hole pocket closes shortly before Z . This leads to two hole pockets at the Z point, being mostly of Fe $3d_{xy}$, $3d_{xz/yz}$ character. Around the \bar{M} point, we observe very small hole pockets with Fe $3d_{xy}$, $3d_{xz/yz}$ character, where the bands with mostly Fe $3d_{xz/yz}$ character are very shallow right above E_F , which leads to a high sensibility to input parameters and total electron charge in the calculation.

By including the spin-orbit interaction we observe an overall repulsion between touching or degenerate bands, which leads to clear separation of the hole pockets along the high symmetry directions (see Fig. 1 (c), (d)).

Comparing these DFT results to ARPES measurements [13, 15, 16] we find that the agreement in size and shape of the hole pockets along the high symmetry directions is quite poor. This disagreement has already been noted in the above cited publications. The inner two pockets (α , ζ) are too large while the outer one (β) is too small. The topology of the Fermi surface also differs from experimental observations. ARPES clearly shows a separated outer hole cylinder at Γ , while the two inner ones overlap considerably [13, 15, 16]. The closure of

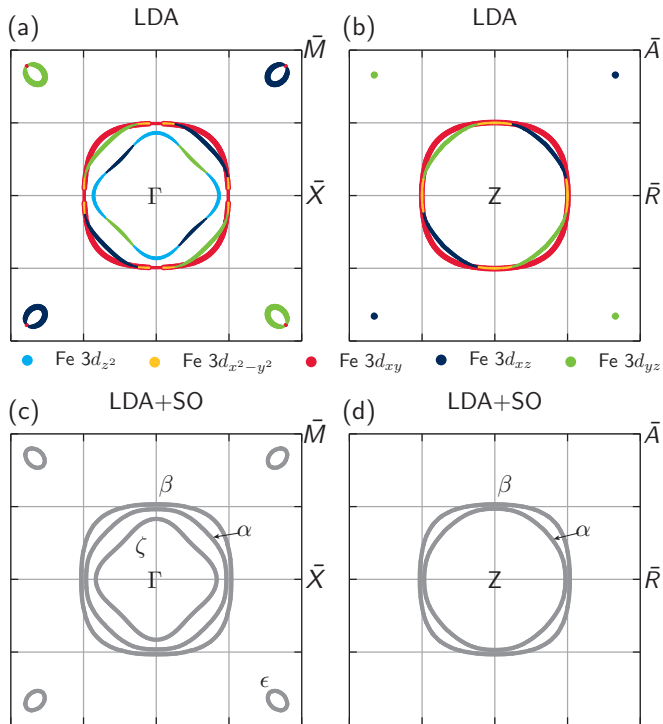


FIG. 1: (Color online) Overview of Fermi surface cuts at $k_z = 0$ and $k_z = \pi$ in KFe_2As_2 obtained from DFT using the LDA exchange correlation functional with and without spin-orbit coupling (SO). Inclusion of spin-orbit coupling only leads to small quantitative changes, in particular a lifting of all apparent degeneracies of Fermi surface sheets. Fermi surfaces are shown in the two-Fe Brillouin zone representation.

the inner hole cylinder is not seen in ARPES [13, 15, 16] or dHvA [12, 17] measurements, leading to a third inner hole pocket at Z in experiments. Also, the hole pockets (ϵ) close to \bar{M} are too small in DFT.

When including correlations on the Fe $3d$ orbitals via DMFT, the electronic structure of KFe_2As_2 changes significantly. Dynamical mean-field theory yields very similar results for both LDA and GGA initial calculations of the electronic structure. In what follows we present the LDA+DMFT results. In the band structure shown in Fig. 2 we observe a strong renormalization of the bands around the Fermi level, with mass enhancements for the Fe $3d$ orbitals ranging from 1.56 to 2.72, as shown in Table I.

These results are in agreement with a previous LDA+DMFT study [18], but still very different from experimentally reported mass enhancements, that can reach values of up to 24 for the small pockets (ϵ) and up to 6.9 for the large pockets (α, β, ζ) in the center of the reciprocal unit cell [12, 17]. It was pointed out in Ref. [17] that flattening of the bands near the Fermi level caused by coupling to low-energy bosonic excitations [36] also contributes to mass enhancements, but may not be accounted for in the DMFT method.

We also observe a reordering of bands along the high

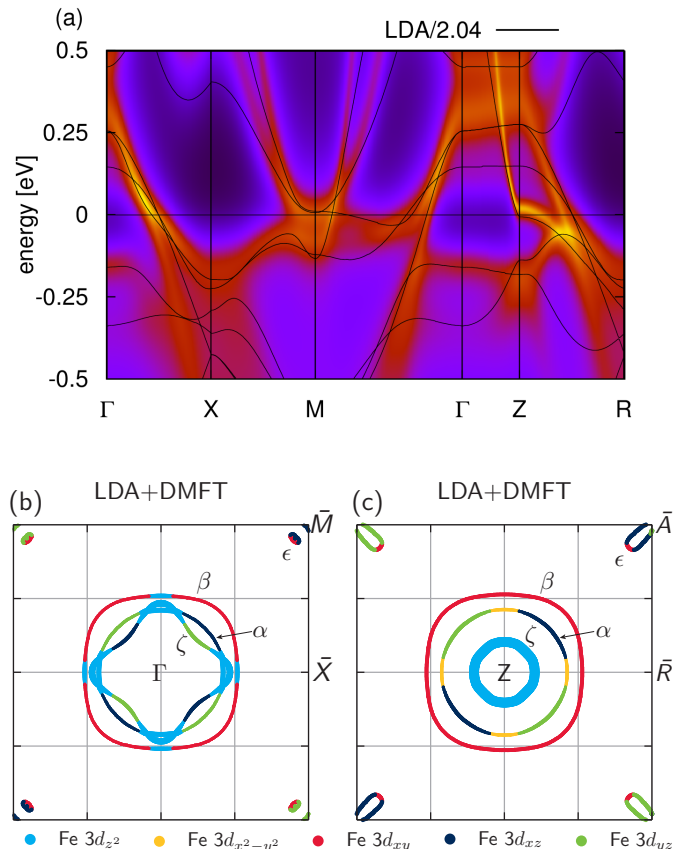


FIG. 2: (Color online) The k -resolved spectral function and orbital-resolved Fermi surface of KFe_2As_2 within LDA+DMFT (see detailed explanation in the text). The LDA bands (black lines) are rescaled by the average mass enhancement of 2.04 for comparison. Dominant orbital characters are indicated by the color scale. Fermi surfaces are shown in the two-Fe Brillouin zone representation.

symmetry directions with significant changes in the size of the hole cylinders. Both the inner sheets (α, ζ) at the Γ point shrink in size, while the outer one (β) gets enlarged, as seen in the LDA+DMFT Fermi surface in Fig. 2. This is in better agreement to the experimental observations. Moreover, we observe a small overlap of the center (ζ) and middle hole pocket (α) with small intersection nodes around Γ , which are also observed in ARPES but were absent in the DFT calculation and previous LDA+DMFT studies [18]. Most importantly, at the Z -point the band of mostly $3d_{z^2}$ character that was located just below the Fermi level is pushed above E_F due to correlations, opening the hole cylinder that was

Orbital	d_{xy}	d_{z^2}	$d_{x^2-y^2}$	$d_{xz/yz}$
$\frac{m^*}{m_{LDA}}$	2.72	1.89	1.56	2.02

TABLE I: The orbital-resolved mass enhancements for the Fe $3d$ orbitals in KFe_2As_2 .

previously closed in the DFT calculation. By also investigating the structure from Rosza and Schuster [26], we found a strong dependence of the shape of this hole pocket on the As- z position (see Appendix). Within DFT alone, an opening of a new hole pocket can be observed by increasing the As height above the Fe plane. Since the band in question originates from the hybridization of Fe 3d with As 4p states, it is extremely sensitive to the arsenic position. The LDA+DMFT middle hole pocket around Z reduces in size compared to LDA, forming an almost k_z -dispersionless hole cylinder between the Γ and Z points. In Figs. 3 and 4 we show three-dimensional plots of the hole cylinders throughout the Brillouin zone.

Recent ARPES experiments [13, 15, 16] and dHvA measurements [12, 17] also observe three hole pockets at the Z point, agreeing well with our calculations. The strong Fe $3d_{z^2}$ character around Z reported from ARPES [16] is also reproduced by our calculation. A detailed comparison shows, however, still some differences between theory and ARPES experiment: the size of the middle hole pocket at both the Γ and Z points is smaller in ARPES, while the inner pocket at Z seems to be larger compared to our results.

The small hole pockets at the \bar{M} point emerge from the crossing of two bands at an energy of about 5 meV above E_F , with very weak dispersion of one of the bands. Therefore, these pockets are extremely sensitive to the Fermi level which makes them strongly dependent on the details of the calculation like the double-counting scheme or the chosen DFT functional. On the experimental side this indicates a strong dependence on the actual composition and possible impurities in the sample; this is a possible explanation for the different sizes of these pockets in ARPES experiments [13, 15, 16]. In our calculations, we carefully checked the results for different double-counting procedures and analytic continuation methods and found overall qualitatively good agreement. Finally, we note that in order to obtain a better agreement with experiment, the middle hole cylinder would have to be shifted inside of the inner cylinder in our calculations. This cannot be achieved by inclusion of local correlations only.

The Fermi surface obtained from LDA+DMFT offers a natural explanation for the magnetic breakdown junctions between orbits α and ζ observed by Terashima *et al.* [12, 17]. Therefore we conclude that the degeneracy of the lines found in ARPES might be due to both experimental resolution and overestimation of the distance between sheets in our calculation. Furthermore we would like to point out that our Fermi surface strongly resembles the octet line-node structure observed in laser ARPES measurements of the superconducting order parameter [6].

B. De Haas-van Alphen effect

Comparing our findings to measurements of quantum oscillations [17] we can confirm that DFT is not able

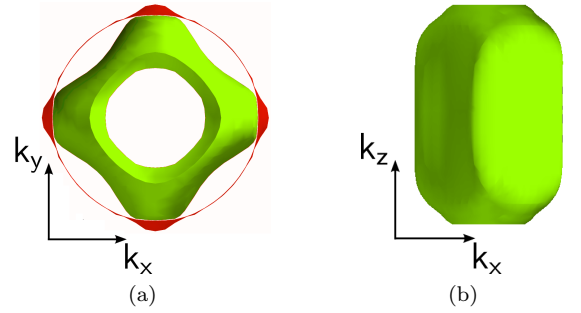


FIG. 3: (Color online) Three dimensional view of the Fermi surface obtained from LDA+DMFT in the two-Fe Brillouin zone representation. Figure (a) shows the intersection nodes between the inner (green) and middle (red) Fermi surface sheet. The configuration used in calculating de Haas-van Alphen frequencies is indicated by the colors. Figure (b) shows the dispersion of the inner Fermi surface sheet along the k_z -axis.

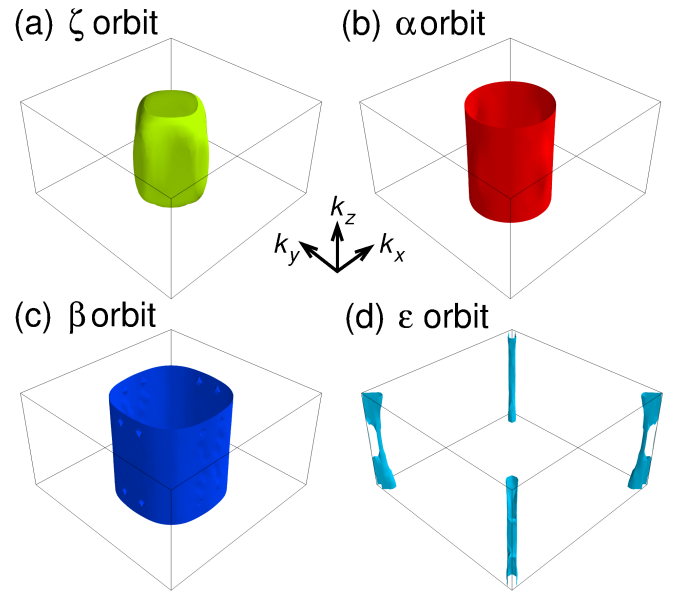


FIG. 4: Three dimensional view of the Fermi surface obtained from LDA+DMFT in the two-Fe Brillouin zone representation. Figure (a) shows the sheet that we attribute to the α orbit observed in de Haas-van Alphen experiments. Figure (b) shows the cylinder attributed to the ζ orbit. Figure (c) shows the cylinder attributed to the β orbit. The small cusps are artifacts from the technical procedure that we carefully exclude in de Haas-van Alphen calculations. Figure (d) shows the sheets that we attribute to the ϵ orbits.

to describe the Fermi surface of KFe_2As_2 correctly. An overview of our results is presented in Fig. 5. LDA and LDA+SO calculations for the structure by Rosza and Schuster are given in the Appendix. They reproduce the DFT results by Terashima *et al.* [12, 17].

The two inner hole pockets (α , ζ) around the Γ point are too large compared to experimental frequencies, while the outermost hole pocket (β) is too small (Fig. 5 left

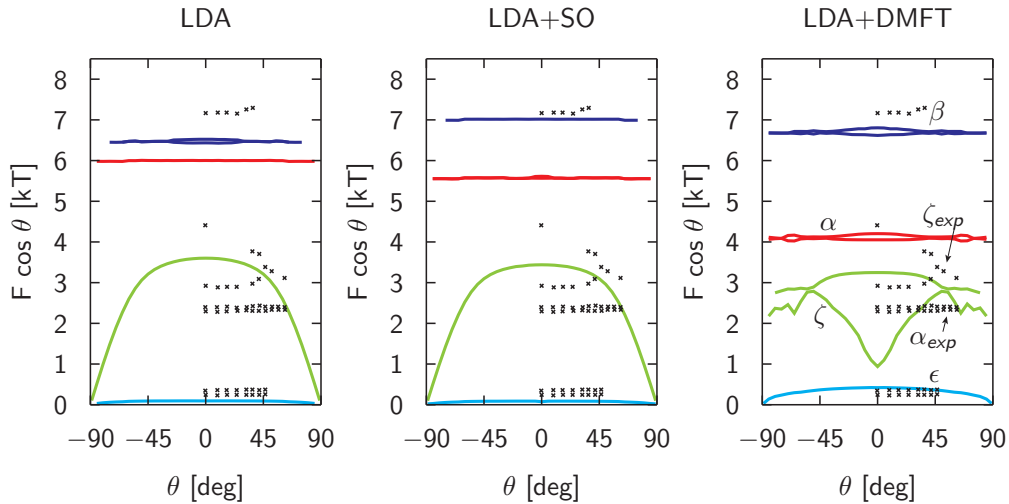


FIG. 5: (Color online) Overview of de Haas-van Alphen frequencies in KFe_2As_2 calculated from density functional theory and dynamical mean-field theory. Lines represent our calculations, while crosses represent experimental frequencies taken from Ref. 17. Color coding is the same as in Fig. 4. The ζ -orbit (innermost) is shown in green, while the frequencies originating from the middle sheet (α) are shown in red. The outermost orbits (β , ϵ) are drawn in blue.

panel). The size of the hole pocket close to \bar{M} (ϵ) is already well described in DFT. Adding spin-orbit coupling already shows the correct tendency to increase the size of the outer hole pocket and decrease the size of the two inner hole pockets. Deviations from experimentally observed frequencies are nevertheless large (Fig. 5 middle panel). The good agreement with experiment for the largest and smallest frequencies comes with persisting disagreement for the two intermediate frequencies.

In the LDA+DMFT calculation (Fig. 5 right panel) the two innermost orbits (α, ζ) intersect around the Γ point (Fig. 2). For the analysis of the dHvA frequencies we take into account the outermost and innermost possible configuration of these two orbits as shown in Fig. 4. The same configuration was attributed to fundamental frequencies observed in dHvA experiment [12, 17]. The outer hole pocket (β) is considerably enlarged. As the corresponding electronic band is flattened, it becomes susceptible to tiny energy shifts. Both inner hole pockets (α, ζ) are shifted to lower frequencies and thus decreased in size. The small orbit (ϵ) close to \bar{M} is enlarged around the Z point, but decreases in size around Γ as shown in Fig. 2. Therefore we only find the maximum frequency for this sheet.

We would like to note that quantum oscillation experiments [37] and ARPES [13, 16] reported the existence of a fourth very small pocket centered at the Z point which was not seen in our calculations for the most recent structure. This fourth pocket is however present in the DFT calculation when using the structure from Rosza and Schuster [26], but we found it to vanish when adding correlations in LDA+DMFT, depending on the double-counting (see Appendix).

The closing of the innermost hole pocket ζ is clearly observed in the LDA+DMFT calculated dHvA frequen-

TABLE II: De Haas-van Alphen frequencies in kT (kiloTesla) for $B \parallel (001)$ obtained from DMFT calculations compared to experimental values [17].

	ϵ_l	ϵ_h	α_l	α_h	ζ_l	ζ_h	β_l	β_h
exp.	0.24	0.36	2.30	2.39	2.89	4.40	7.16	-
LDA+DMFT	-	0.42	4.05	4.20	0.94	3.25	6.62	6.81

TABLE III: Electron orbit averaged effective masses in m_e for $B \parallel (001)$ obtained from DMFT calculations compared to experimental values [17].

	ϵ_Γ	ϵ_Z	α_Γ	α_Z	ζ_Γ	ζ_Z	β_Γ	β_Z
exp.	6.0	7.2	6.0	6.5	8.5	18.0	19.0	19.0
LDA+DMFT	-	5.9	3.4	4.6	2.4	5.3	8.3	8.3

cies by the appearance of a lower extremal frequency. As pointed out before in the ARPES section, the middle hole cylinder would have to be decreased in size considerably to match the experimental frequencies. This would in turn increase the enclosed volume of the sheet labeled ζ and thus shift it toward experimentally observed values. A comparison of experimental and LDA+DMFT frequencies for $B \parallel (001)$ is given in Table II.

Furthermore we calculated effective masses averaged over extremal orbits on the Fermi surface from the LDA+DMFT excitation energies. These masses correspond to the effective masses observed in dHvA experiments (Table III). Note that values given in this table are *absolute* masses in contrast to mass *enhancements* given in Table I.

Qualitatively our calculation captures the trends that

are observed in sheet-resolved effective masses, however we certainly miss effects originating from other than electron-electron interactions, which increase effective masses seen in dHvA experiments such as electron-phonon coupling.

IV. CONCLUSION

In this paper we presented combined density functional theory with dynamical mean-field theory calculations of the Fermi surface and de Haas-van Alphen frequencies in KFe_2As_2 . We first showed that DFT calculations with LDA or GGA exchange correlation functionals, with or without spin-orbit coupling fail to reproduce the experimentally observed electronic structure of KFe_2As_2 .

Most notably, DFT predicts no third inner hole pocket at the Z point, which we find to open in our LDA+DMFT calculation in agreement with experiment. We also obtain a qualitatively correct k_z dispersion of the iron bands, where between the Γ and Z points the dispersion of the inner hole cylinder is greatly increased with almost no dispersion of the middle hole cylinder, giving a much better agreement with dHvA measurements when identifying them in different order in experiment.

The intersection nodes we found on the inner two hole cylinders offer a natural explanation for magnetic breakdown orbits observed in dHvA measurements (Ref. 17).

The obtained effective mass-enhancements about 1.6 – 2.7 show that KFe_2As_2 is a moderately correlated metal and thus a DFT calculation fails to capture the important features that lead to the experimentally observed electronic structure. This has strong implications for the obtained dHvA frequencies, where LDA+DMFT gives distinctively different results than DFT. Our results are in better agreement with both ARPES (Refs. 13, 16) and quantum oscillation (Refs. 12, 17) experiments. The observed strong flattening of electronic bands gives a possible explanation for the spread of experimental results in this compound in terms of extreme sensitivity to the experimental stoichiometry. We conclude that LDA+DMFT captures most of the important correlation effects in KFe_2As_2 and such a treatment may be necessary in order to understand the controversial nature of superconductivity in this system. This will be a subject of future work.

Acknowledgments

The authors would like to thank Milan Tomić, Markus Aichhorn, Emanuel Gull, Luca de Medici, Peter J. Hirschfeld, Amalia Coldea and Kristjan Haule for useful discussions and suggestions and gratefully acknowledge financial support by the Deutsche Forschungsgemeinschaft through grant SPP 1458. Daniel Guterding acknowledges support by the German National Academic Foundation.

Appendix A: Sensitivity analysis of the Fermi surface and de Haas-van Alphen frequencies

Previous theoretical works on KFe_2As_2 were based on the structural data obtained by Rosza and Schuster [26], while new results also for higher pressures became recently available by Tafti *et al.* [25]. These structures differ most noticeably in the As z -position, where the old structure has a fractional coordinate of $z = 0.1475$, while the new one yields $z = 0.140663$ by interpolation to 0 GPa. Therefore, to interpret current theoretical investigations correctly, we investigate the dependence of the Fermi surface and de Haas-van Alphen frequencies of KFe_2As_2 on the two different structures and also on different double-counting methods within LDA+DMFT. We also tested the dependence of these quantities upon considering LDA versus GGA and found very minor changes. Here we present GGA results.

We find very different behavior for the two structural configurations: The Fermi surfaces for the Rosza and Schuster [26] structure can be seen in Fig. 6, to be compared to the Tafti *et al.* [25] structure in Fig. 1. The cut at $k_z = 0$ is qualitatively identical but the Fermi surface topology at the Z -point is different, where the structure of Rosza and Schuster with the higher As z -position features two additional inner hole pockets around Z . The inner one emerges from a small hole pocket centered at Z , while the second inner one corresponds to the open ζ -hole cylinder, which closes shortly before $k_z = \pi$ in the structure by Tafti *et al.* [25]. From our calculations we can deduce that the As z -position is the key factor for the existence of these hole pockets. This makes sense since their main orbital character is either Fe $3d_{z^2}$ or As $4p$, giving rise to a strong dependence on the Fe-As bonding distance. By lowering the As z -position, and thus enhancing the hybridization of the Fe $3d$ with the As $4p$ orbitals, the two inner pockets become smaller and finally vanish.

In Fig. 7 we show cuts of the Fermi surface in LDA+DMFT, calculated for the structure by Rosza and Schuster. The electronic structure depends on the double-counting correction, where with the FLL double-counting the fourth inner hole pocket stays present at the Z point, whereas with the around mean-field (AMF) double-counting it vanishes. This can be explained by the large As $4p$ character of the inner hole pocket, which makes it sensible to the double-counting method. Since AMF reduces the self-energy by a smaller degree than FLL, this band is pushed below the Fermi level when using the AMF method. In the structure by Tafti *et al.* this band is further below the Fermi level already in the DFT calculation, lowering the As $4p$ contribution to the density of states at E_F . Therefore, we see only slight differences between the two double-counting corrections in the Tafti *et al.* structure with no qualitative changes.

In Fig. 8 we show the dHvA frequencies for the structure by Rosza and Schuster. The small orbits at the \bar{M} -point are not shown as they give very low frequencies.

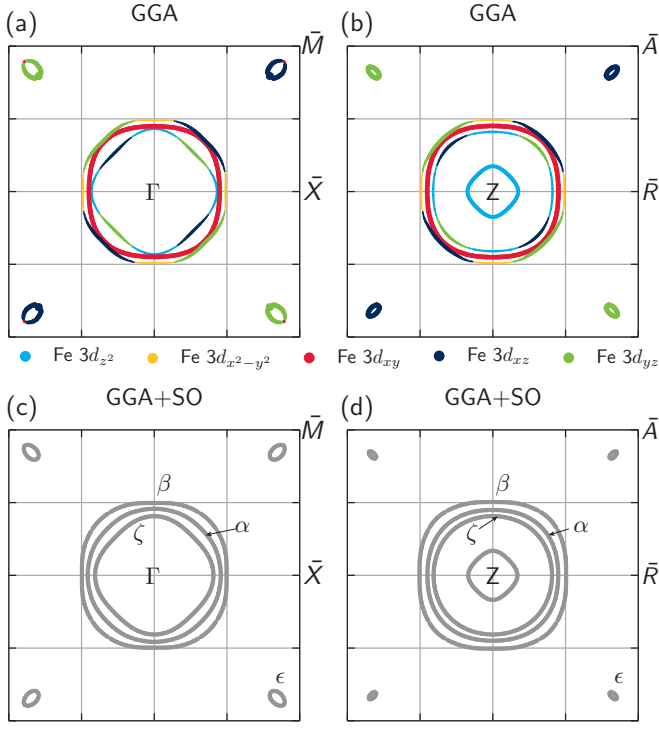


FIG. 6: (Color online) The orbital-resolved Fermi surface of KFe_2As_2 within DFT for the structural data by Rosza and Schuster [26]. Dominant orbital characters are indicated by the color scale. Fermi surfaces are shown in the two-Fe Brillouin zone representation.

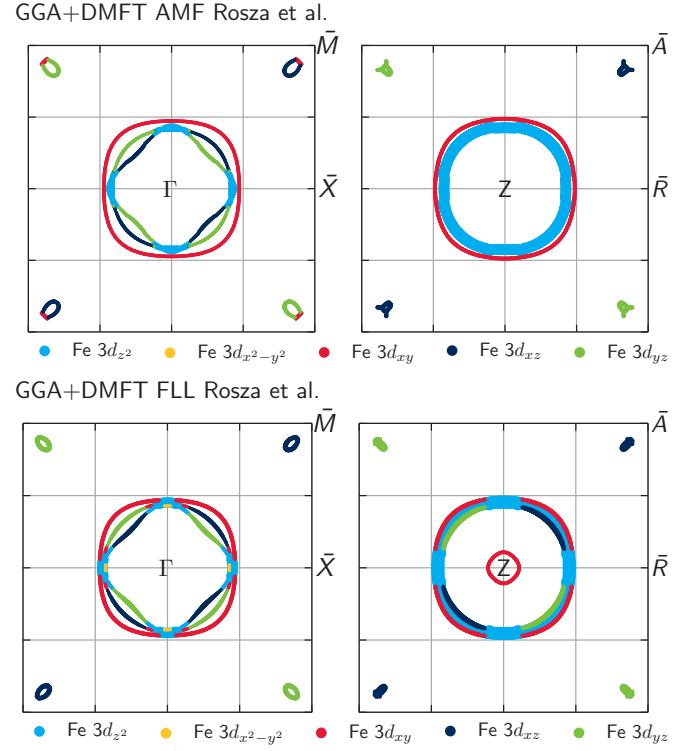


FIG. 7: (Color online) The orbital-resolved Fermi surface of KFe_2As_2 within GGA+DMFT using the structural data by Rosza and Schuster [26]. Dominant orbital characters are indicated by the color scale. Fermi surfaces are shown in the two-Fe Brillouin zone representation. AMF indicates the around mean-field, FLL the fully-localized limit double-counting.

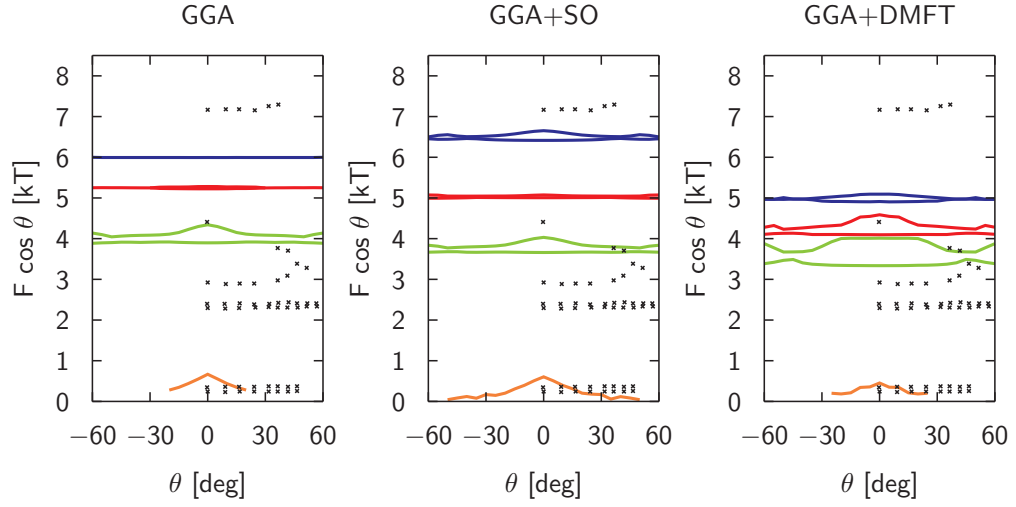


FIG. 8: (Color online) Overview of de Haas-van Alphen frequencies in KFe_2As_2 calculated from density functional theory and dynamical mean-field theory with FLL double-counting using the structural data by Rosza and Schuster [26]. Lines represent our calculations, while crosses represent experimental frequencies taken from Ref. 17. Color coding is the same as in Fig. 4. The ζ -orbit (innermost) is shown in green, while the frequencies originating from the middle sheet (α) are shown in red. The outermost orbits (β , ϵ) are drawn in blue. The orbit shown in orange corresponds to a small pocket at the Z -point.

-
- [1] M. Rotter, M. Pangerl, M. Tegel, D. Johrendt, *Superconductivity and Crystal Structures of $(\text{Ba}_{1-x}\text{K}_x)\text{Fe}_2\text{As}_2$ ($x = 0-1$)*, *Angew. Chem. Int. Ed.* **47**, 7949 (2008).
- [2] K. Kihou, T. Saito, S. Ishida, M. Nakajima, Y. Tomioka, H. Fukazawa, Y. Kohori, T. Ito, S. Uchida, A. Iyo, C. H. Lee, and H. Eisaki, *Single Crystal Growth and Characterization of the Iron-Based Superconductor KFe_2As_2 Synthesized by KAs Flux Method*, *J. Phys. Soc. Jpn.* **79**, 124713 (2010).
- [3] F. Wang, D.-H. Lee, *The electron pairing mechanism of iron-based superconductors*, *Science* **332**, 200-204 (2011).
- [4] P. J. Hirschfeld, M. M. Korshunov, I. I. Mazin, *Gap symmetry and structure of Fe-based superconductors* *Rep. Prog. Phys.* **74**, 124508 (2011).
- [5] A. V. Chubukov, *Pairing mechanism in Fe-based superconductors*, *Annu. Rev. Condens. Matter Phys.* **3**, 57-92 (2012).
- [6] K. Okazaki, Y. Ota, Y. Kotani, W. Malaeb, Y. Ishida, T. Shimojima, T. Kiss, S. Watanabe, C.-T. Chen, K. Kihou, C. H. Lee, A. Iyo, H. Eisaki, T. Saito, H. Fukazawa, Y. Kohori, K. Hashimoto, T. Shibauchi, Y. Matsuda, H. Ikeda, H. Miyahara, R. Arita, A. Chainani, and S. Shin, *Octet-Line Node Structure of Superconducting Order Parameter in KFe_2As_2* , *Science* **337**, 1314 (2012).
- [7] R. Thomale, Ch. Platt, W. Hanke, J. Hu, B. A. Bernevig, *Exotic d-Wave Superconducting State of Strongly Hole-Doped $\text{K}_x\text{Ba}_{1-x}\text{Fe}_2\text{As}_2$* , *Phys. Rev. Lett.* **107**, 117001 (2011).
- [8] J.-Ph. Reid, M. A. Tanatar, A. Juneau-Fecteau, R. T. Gordon, S. René de Cotret, N. Doiron-Leyraud, T. Saito, H. Fukazawa, Y. Kohori, K. Kihou, C. H. Lee, A. Iyo, H. Eisaki, R. Prozorov, and L. Taillefer, *Universal Heat Conduction in the Iron Arsenide Superconductor KFe_2As_2 : Evidence of a d-Wave State*, *Phys. Rev. Lett.* **109**, 087001 (2012).
- [9] S. Maiti, M. M. Korshunov, T. A. Maier, P. J. Hirschfeld, A. V. Chubukov, *Evolution of the Superconducting State of Fe-Based Compounds with Doping*, *Phys. Rev. Lett.* **107**, 147002 (2011).
- [10] K. Suzuki, H. Usui, and K. Kuroki, *Spin fluctuations and unconventional pairing in KFe_2As_2* , *Phys. Rev. B* **84**, 144514 (2011).
- [11] F. F. Tafti, A. Juneau-Fecteau, M.-È. Delage, S. René de Cotret, J.-Ph. Reid, A. F. Wang, X.-G. Luo, X. H. Chen, N. Doiron-Leyraud, and L. Taillefer, *Sudden reversal in the pressure dependence of T_c in the iron-based superconductor KFe_2As_2* , *Nature Physics* **9**, 349 (2013).
- [12] T. Terashima, M. Kimata, N. Kurita, H. Satsukawa, A. Harada, K. Hazama, M. Imai, A. Sato, K. Kihou, C.-H. Lee, H. Kito, H. Eisaki, A. Iyo, T. Saito, H. Fukazawa, Y. Kohori, H. Harima, and S. Uji, *Fermi Surface and Mass Enhancements in KFe_2As_2 from de Haas-van Alphen Effect Measurements*, *J. Phys. Soc. Jpn.* **79**, 053702 (2010).
- [13] T. Yoshida, I. Nishi, A. Fujimori, M. Yi, R. G. Moore, D.-H. Lu, Z.-X. Shen, K. Kihou, P. M. Shirage, H. Kito, C. H. Lee, A. Iyo, H. Eisaki, and H. Harima, *Fermi surfaces and quasi-particle band dispersions of the iron pnictide superconductor KFe_2As_2 observed by angle-resolved photoemission spectroscopy*, *Journal of Physics and Chemistry of Solids* **72**, 465 (2011).
- [14] M. Kimata, T. Terashima, N. Kurita, H. Satsukawa, A. Harada, K. Kodama, K. Takehana, Y. Imanaka, T. Takamasu, K. Kihou, C.-H. Lee, H. Kito, H. Eisaki, A. Iyo, H. Fukazawa, Y. Kohori, H. Harima, and S. Uji, *Cyclotron Resonance and Mass Enhancement by Electron Correlation in KFe_2As_2* , *Phys. Rev. Lett.* **107**, 166402 (2011).
- [15] T. Sato, N. Nakayama, Y. Sekiba, P. Richard, Y.-M. Xu, S. Souma, T. Takahashi, G. F. Chen, J. L. Luo, N. L. Wang, and H. Ding, *Band Structure and Fermi Surface of an Extremely Overdoped Iron-Based Superconductor KFe_2As_2* , *Phys. Rev. Lett.* **103**, 047002 (2009).
- [16] T. Yoshida, S. Ideta, I. Nishi, A. Fujimori, M. Yi, R. G. Moore, S. K. Mo, D.-H. Lu, Z.-X. Shen, Z. Hussain, K. Kihou, P. M. Shirage, H. Kito, C. H. Lee, A. Iyo, H. Eisaki, and H. Harima, *Orbital-dependent electron correlation effect on the two- and three-dimensional Fermi surfaces in KFe_2As_2 revealed by angle-resolved photoemission spectroscopy*, arXiv:1205.6911 (unpublished).
- [17] T. Terashima, N. Kurita, M. Kimata, M. Tomita, S. Tsuchiya, M. Imai, A. Sato, K. Kihou, C.-H. Lee, H. Kito, H. Eisaki, A. Iyo, T. Saito, H. Fukazawa, Y. Kohori, H. Harima, and S. Uji, *Fermi surface in KFe_2As_2 determined via de Haas-van Alphen oscillation measurements*, *Phys. Rev. B* **87**, 224512 (2013).
- [18] Z. P. Yin, K. Haule, G. Kotliar, *Kinetic frustration and the nature of the magnetic and paramagnetic states in iron pnictides and iron chalcogenides*, *Nature Mater.* **10**, 932 (2011).
- [19] M. Aichhorn, S. Biermann, T. Miyake, A. Georges, and M. Imada, *Theoretical evidence for strong correlations and incoherent metallic state in FeSe* , *Phys. Rev. B* **82**, 064504 (2010).
- [20] P. Hansmann, R. Arita, A. Toschi, S. Sakai, G. Sangiovanni, and K. Held, *Dichotomy between Large Local and Small Ordered Magnetic Moments in Iron-Based Superconductors*, *Phys. Rev. Lett.* **104**, 197002 (2010).
- [21] M. Aichhorn, L. Pourovskii, and A. Georges, *Importance of electronic correlations for structural and magnetic properties of the iron pnictide superconductor LaFeAsO* , *Phys. Rev. B* **84**, 054529 (2011).
- [22] J. Ferber, K. Foyevtsova, R. Valentí, and H. O. Jeschke, *LDA + DMFT study of the effects of correlation in LiFeAs* , *Phys. Rev. B* **85**, 094505 (2012).
- [23] J. Ferber, H. O. Jeschke, and R. Valentí, *Fermi Surface Topology of LaFePO and LiFeP* , *Phys. Rev. Lett.* **109**, 236403 (2012).
- [24] P. Werner, M. Casula, T. Miyake, F. Aryasetiawan, A. J. Millis and Silke Biermann, *Satellites and large doping and temperature dependence of electronic properties in hole-doped BaFe_2As_2* , *Nature Physics* **8**, 331 (2012).
- [25] F. F. Tafti, J. P. Clancy, M. Lapointe-Major, C. Colignon, S. Faucher, J. Sears, A. Juneau-Fecteau, N. Doiron-Leyraud, A. F. Wang, X. G. Luo, S. Desgreniers, Young-June Kim, X. H. Chen, and Louis Taillefer, *Sudden reversal in the pressure dependence of T_c in the iron-based superconductor CsFe_2As_2 : A possible link between inelastic scattering and pairing symmetry* arXiv:1403.0110 (unpublished).
- [26] S. Rosza, H. U. Schuster, *Z. Naturforsch. B* **36**, 1668 (1981).
- [27] P. Blaha, K. Schwarz, G. K. H. Madsen, D. Kvasnicka, and J. Luitz 2001 WIEN2k, *An Augmented*

- PlaneWave+LocalOrbitals Program for Calculating Crystal Properties* (Karlheinz Schwarz, Techn. Universität Wien, Austria).
- [28] J. P. Perdew, K. Burke, M. Ernzerhof, *Generalized Gradient Approximation Made Simple*, Phys. Rev. Lett. **77**, 3865 (1996).
 - [29] M. Aichhorn, L. Pourovskii, V. Vildosola, M. Ferrero, O. Parcollet, T. Miyake, A. Georges, S. Biermann, *Dynamical mean-field theory within an augmented plane-wave framework: Assessing electronic correlations in the iron pnictide LaFeAsO*, Phys. Rev. B **80**, 085101 (2009).
 - [30] B. Bauer et al. (ALPS Collaboration), *The ALPS project release 2.0: open source software for strongly correlated systems*, J. Stat. Mech. P05001 (2011).
 - [31] L. Boehnke, H. Hafermann, M. Ferrero, F. Lechermann, O. Parcollet, *Orthogonal polynomial representation of imaginary-time Green's functions*, Phys. Rev. B **84**, 075145 (2011).
 - [32] H. Hafermann, K. R. Patton, P. Werner, *Improved estimators for the self-energy and vertex function in hybridization-expansion continuous-time quantum Monte Carlo simulations*, Phys. Rev. B **85**, 205106 (2012).
 - [33] K. S. D. Beach, *Identifying the maximum entropy method as a special limit of stochastic analytic continuation*, arXiv:cond-mat/0403055 (unpublished).
 - [34] P. M. C. Rourke, S. R. Julian, *Numerical extraction of de Haas-van Alphen frequencies from calculated band energies*, Comput. Phys. Commun. **183**, 324 (2012).
 - [35] F. Lekien, J. Marsden, *Tricubic interpolation in three dimensions*, Int. J. Numer. Meth. Engng. **63**, 455–471 (2005).
 - [36] L. Ortenzi, E. Cappelluti, L. Benfatto, and L. Pietronero, *Fermi-Surface Shrinking and Interband Coupling in Iron-Based Pnictides*, Phys. Rev. Lett **103**, 046404 (2009).
 - [37] D. A. Zocco, K. Grube, F. Eilers, T. Wolf, H. v. Löhneysen, *Fermi Surface of KFe₂As₂ from Quantum Oscillations in Magnetostriction*, arXiv:1401.4403 (unpublished).